



1 **Changes in the shape of cloud ice water content vertical**
2 **structure due to aerosol variations**

3

4 **Steven T. Massie^{1,3}, Julien Delanoë², and Charles G. Bardeen³**

5

6 [1]{Laboratory for Atmospheric and Space Physics, Boulder, Colorado}

7 [2]{LATMOS/IPSL/UVSQ, Guyancourt, France}

8 [3]{National Center for Atmospheric Research, Boulder, Colorado}

9 Correspondence to: S. T. Massie (Steven.Massie@lasp.colorado.edu)

10

11 **Abstract**

12 Changes in the shape of cloud ice water content vertical structure due to aerosol
13 variations are calculated in the Tropics during 2007-2010 based upon an analysis of
14 DARDAR ice water content (IWC) profiles for deep convective clouds. DARDAR
15 profiles are a joint retrieval of CloudSat-CALIPSO data. Our analysis is performed for 12
16 separate regions over land and ocean, and carried out applying Moderate-Resolution
17 Imaging Spectroradiometer (MODIS) aerosol optical depth (AOD) fields that attempt to
18 correct for 3D cloud adjacency effects. The 3D cloud adjacency effects have a small
19 impact upon our calculations of aerosol-cloud indirect effects. IWC profiles are averaged
20 for three AOD bins individually for the 12 regions. The IWC average profiles are also
21 normalized to unity at 5 km altitude in order to study changes in the shape of the average
22 IWC profiles as AOD increases. Derivatives of the IWC average profiles, and
23 derivatives of the IWC shape profiles, in percent change per 0.1 change in MODIS AOD
24 units, are calculated separately for each region. Means of altitude-specific probability



1 distribution functions, which include both ocean and land IWC shape regional
2 derivatives, are modest, near 5%, and positive to the 2σ level between 11 and 15 km
3 altitude.

4

5 **1 Introduction**

6 Uncertainty in aerosol effects upon clouds remains the largest of the global climate
7 forcing uncertainties (Stocker et al., 2013). Tao et al. (2012) discuss the various types of
8 aerosol indirect effects (e.g. effects on cloud droplets and ice particles, reflectance, cloud
9 heights, lifetime, coverage, and precipitation). Though various aerosol indirect effects
10 have been identified, there remains much quantitative uncertainty.

11 By the cloud invigoration mechanism (Rosenfeld et al., 2008), an increase in aerosol is
12 expected to modify the manner in which vertical and horizontal cloud structure develops
13 in deep convective clouds. The cloud invigoration mechanism is of fundamental
14 importance in regard to aerosol indirect effects upon deep convective clouds. It is
15 expected that the vertical ice water content (IWC), particle radii, and heating rate profiles
16 of a deep convective cloud differs under low and high aerosol optical depths (AODs) due
17 to different initial cloud condensation nuclei (CCN) values in the lower portion of the
18 cloud. A change in the CCN concentration alters the formation rate and size of liquid
19 droplets, allowing more water to be transported above the freezing level, which leads to a
20 perturbed vertical profile of latent heat release, and subsequent invigoration of cloud
21 development. This invigoration effect will occur throughout the cloud, changing IWC
22 vertical structure.

23 The literature of observed and modeled aerosol indirect effects, however, is characterized
24 by a variety of conclusions with differences in even the *sign* of the effects. For example,
25 Koren et al. (2010) analyzed Moderate-Resolution Imaging Spectroradiometer (MODIS)
26 AOD and cloud top pressure data for July – August 2007 over the Atlantic west of
27 equatorial Africa for low and high clouds. For high clouds near 370 hPa (i.e. 7 km
28 altitude, see Figure 6 of Koren et al., 2010), cloud top pressure changed by -7% / 0.1



1 AOD (i.e. cloud top heights *increased* as AOD increased). In this paper we use % change
2 per 0.1 AOD units in order to compare the calculations from several studies. Assuming
3 that the cloud top position is dependent upon the location of cloud vertical optical depths
4 near unity, a decrease in cloud top pressure corresponds to moving the optical depth
5 profile upwards in altitude. IWC is then +7% / 0.1 AOD larger at the position of the
6 higher cloud top. In contrast, Wall, Zipser, and Liu (2014) studied congestus (4-8 km
7 altitude range), analyzing 14 years of Tropical Rainfall Measuring Mission (TRMM)
8 radar precipitation features, and 6 years of CloudSat radar reflectivity data. Aerosol Index
9 (AI) data (i.e. AI is the product of MODIS AOD and the MODIS Angstrom exponent)
10 were collocated with the TRMM and CloudSat data. TRMM echo-top heights *increased*
11 with increasing AI over the Amazon and Africa, and *decreased* over the equatorial
12 Atlantic and southwest United States. Differences in CloudSat maximum reflectivity
13 means of clean and dirty congestus were statistically significant at the 99% level below 4
14 km over the Amazon, and at 4-5 km over Africa, but *not* at higher altitudes.

15 According to theory, buoyancy increases by the release of latent heat, and decreases
16 when condensate loading (i.e. the weight of liquid or ice in a fluid parcel) increases (see
17 Eqns 2.50 – 2.53 of Houze, 2014). Lebo and Seinfeld (2011) state that “the aerosol-
18 induced effect is controlled by the balance between latent heating and the increase in
19 condensed water aloft, each having opposing effects on buoyancy.” Since changes in
20 buoyancy can be positive or negative, depending upon specific situations in which latent
21 heating or condensate perturbations dominant, changes in cloud structure IWC likely
22 could be positive or negative as AOD increases.

23 Lebo and Seinfeld (2011) modeled aerosol effects on deep convection by applying the
24 Weather Research and Forecasting (WRF) model as a cloud resolving model, with
25 separate bulk and bin microphysics schemes. Figure 6 of Lebo and Seinfeld (2011)
26 presents domain averaged liquid and IWC profiles at 2, 4, and 6 hours for “Clean”,
27 “Semi-Polluted”, and “Polluted” scenarios, with cloud condensation nuclei (CCN) values
28 of 100, 200, and 500 cm⁻³, respectively. The three IWC profiles for the three CCN values
29 are equal to each other at 5 (6) km altitude for the bulk (bin) microphysics schemes,
30 respectively, and then diverge at higher altitudes. This diverging characteristic indicates



1 that the shape of the IWC profile changes as AOD changes. This Figure motivates us to
2 calculate IWC average profiles for individual regions in the Tropics, and IWC *shape*
3 profiles, for several AOD bins. The IWC shape profiles are obtained by normalizing the
4 IWC average profiles to unity at 5 km altitude.

5 There are noticeable differences in the bulk and bin microphysics model calculations in
6 Figure 6 of Lebo and Seinfeld (2011). The bulk scheme IWC profiles differ by – 5% at
7 the IWC peak near 6 km altitude, indicating a decrease in IWC as aerosol increases,
8 while the bin microphysics IWC profiles differ by 120% at the IWC peak near 9 km
9 altitude, indicating a large increase in IWC as aerosol increases. Figure 1 of Rosenfeld et
10 al. (2008), which graphs 500 nm AOD as a function of CCN, can be used to estimate
11 AODs that correspond to the model CCN values. The difference in AOD between the
12 Clean and Polluted CCN values is approximately 0.094. The 120% increase in IWC
13 therefore translates to an increase in IWC of 127% per 0.1 AOD. Lebo and Seinfeld
14 (2011) attribute the bulk and bin microphysics model differences to differences in vertical
15 motion and particle size (sedimentation) characteristics of the two microphysical
16 schemes.

17 Storer and van den Heever (2013) modeled deep convective clouds by running the
18 Regional Atmospheric Modeling System (RAMS) (Cotton et al., 2003) in a 2D radiative-
19 convective equilibrium framework. Six CCN loadings between 100 and 3200 cm⁻³ were
20 applied in separate calculations. After a 60 day initialization, model output was sampled
21 every 5 min during a 10 day period. They note that early storm updrafts were influenced
22 by increased latent heating, while more mature updrafts were largely influenced by
23 increased drag from condensate loading. Differences in buoyancy curves for “polluted”
24 and “clean” aerosol cases (see Figure 8 of Storer and van den Heever, 2013) indicate that
25 latent heating effects were numerically smaller, by an order of magnitude, than those due
26 to condensate loading. The number of cloud-top counts, averaged over 10 days, shifted
27 toward higher and medium cloud tops and fewer low cloud tops (see Figure 1 of Storer
28 and van den Heever, 2013). The freezing level was near 4.4 km, with low, medium, and
29 high cloud tops defined for altitudes less than 4.4 km, 4.4-10 km, and altitudes greater
30 than 10 km, respectively. On a percentage basis, medium and high cloud top heights



1 increased by approximately 3% and 5%, respectively, between the 100 and 400 cm⁻³
2 CCN values. The 100 cm⁻³ and 400 cm⁻³ CCN values are closest in value to those used in
3 the Lebo and Seinfeld (2011) calculations discussed above.

4 Changes in the shape of cloud ice water content vertical structure, and changes in ice
5 water content (IWC) vertical profiles, due to aerosol variations, are calculated in this
6 paper for the Tropics over land and oceans during 2007-2010 based upon an analysis of
7 DARDAR IWC profiles of deep convective clouds. DARDAR profiles (Delanoë and
8 Hogan, 2008; Delanoë and Hogan, 2010) are a joint radar-lidar retrieval using CloudSat
9 radar reflectivity and CALIOP lidar observations at 532 nm. We carry out our
10 calculations over several years (2007-2010), individual regions and seasons, in order to
11 build up statistics. Section 2 discusses the data used in our study, Section 3 discusses our
12 Methodology, and results are presented in Section 4. A discussion of the results and
13 conclusions are presented in Section 5.

14

15 **2 Data**

16 Ice water content vertical profiles are from the v2.1.0 DARDAR (raDAR/liDAR) data
17 archive (<http://www.icare.univ-lille1.fr/drupal/archive/>) of the ICARE Thematic Center.
18 The DARDAR cloud product is derived using the Varcloud algorithm (Delanoë and
19 Hogan 2008) and utilizes CloudSat reflectivity, and CALIOP lidar backscatter at 532 nm
20 to jointly retrieve the properties of ice clouds (e.g. IWC, visible extinction, effective
21 cloud particle radius). There is one DARDAR profile, with a vertical resolution of 60 m,
22 for every CloudSat radar profile and therefore an along track horizontal resolution of 1.7
23 km. Cloudsat (Stephens et al, 2002) and the CALIOP lidar (on the CALIPSO satellite,
24 Winker et al., 2010) were launched in tandem in 2006 as part of the A-Train. We analyze
25 data from all months of 2007 through 2010.

26 The DARDAR retrieval algorithm is discussed in Delanoë and Hogan (2008), Delanoë
27 and Hogan (2010) and in ICARE archive documentation (http://www.icare.univ-lille1.fr/drupal/projects_data/dardar/docs/varcloud_algorithm_description-v1.0.pdf). The



1 applied optimal estimation technique (see Rodgers, 2000 for a general discussion)
2 incorporates up to date aircraft particle size distribution and habit information to
3 formulate forward model look-up tables. The lidar forward model uses a fast radiative
4 transfer code (Hogan 2006). The combination of 95 GHz CloudSat radar and 532 nm
5 CALIOP lidar observations provide information on both small and larger ice particles,
6 since CloudSat and CALIOP are sensitive to larger and smaller particles, respectively.
7 Since the lidar is subject to strong attenuation, the radar measurement takes over for thick
8 ice clouds. The radar-lidar overlap region allows one to retrieve simultaneously size and
9 concentration information. For this reason the combination of the two measurements
10 improves the retrieval of cloud properties compared to single instrument retrievals. The
11 DARDAR data focuses upon ice particles, so our analysis is restricted to altitudes above
12 5 km.

13 Deng et al. (2013) found reasonable agreement between CloudSat-CALIPSO (2C-ICE)
14 and DARDAR retrieval products. IWC values from 2B-CWC-RO, 2C-ICE, and
15 DARDAR generally are in good agreement, while 2B-CWC-RVOD radii were 40%
16 larger than the 2C-ICE and DARDAR radii.

17 One stated concern in aerosol-indirect effect studies is that it is difficult to measure
18 aerosol optical depths near clouds using nadir view satellite instruments. A cloud away
19 from an observation point scatters light from the cloud towards the nadir observation
20 point, which is then scattered towards the satellite sensor. Varnai and Marshak (2009)
21 quantified how MODIS reflectance is enhanced as a function of distance to the nearest
22 cloud. The reflectance is enhanced by ~10% when clouds are 5 km away from clear sky
23 footprints at a wavelength of 0.68 μm . Zhang et al. (2005) compared AERONET and
24 MODIS MOD04 AODs. They demonstrate that MODIS AODs are enhanced at cloud
25 edges, with differences between MODIS and AERONET AODs increasing as the cloud
26 fraction increases, while the AERONET values stay relatively constant. We address this
27 concern in our calculations by using the latest V6 MODIS aerosol data that include a
28 parameter indicating the average pixel distance from a measured AOD to the nearest
29 cloud feature.



1 MODIS version 6 MYD04 data files are used to specify daily aerosol optical depth fields.
2 In particular, we utilize the “Optical_Depth_Land_and_Ocean” AOD values at 0.55 μm ,
3 which are specified at 10 km horizontal spatial resolution. We process the 10 km AODs
4 into daily data files at $1^\circ \times 1^\circ$ longitude-latitude resolution for 25° S to 25° N. As
5 discussed by Levy et al. (2013), the Collection 6 (henceforth C6) aerosol retrieval
6 algorithms have made several improvements compared to the C5 data. The C6
7 “Average_Cloud_Pixel_Distance_Land_Ocean” variable specifies the number of pixel
8 units from an AOD to the nearest cloud pixel. Pixel unit distances are on the order of 0.5
9 km. We use this variable to calculate separate $1^\circ \times 1^\circ$ AOD fields for several “cloud
10 screening” cases. For the first case, all AODs are used within a $1^\circ \times 1^\circ$ grid box if the AOD
11 is between 10^{-3} and 3. Another set uses all AODs that are e.g. 2 or more pixel units from
12 MODIS clouds. Daily $1^\circ \times 1^\circ$ fields of AODs for 2, 4, and 6 pixel units, and the “all AOD”
13 case, are calculated separately for 25° S to 25° N. As discussed in the next section, the
14 AOD fields are used in separate calculations, for each pixel-distance case, to assess the
15 sensitivity of the calculations to 3D cloud adjacency effects. The AODs used in our
16 processing are for quality flag 3 (i.e. only the best quality data is used).

17 Levy et al. (2014) discusses the differences in C6 and C5 Aqua MODIS AODs. C6
18 AODs increase by 0.05 over the tropical ocean and the Amazon, decrease by -0.05 over
19 the southern oceans and northern mid-latitudes, and increase by 0.02 on a global basis.
20 C6 AODs over the land increased by 0.10 over East Asia, vegetation, Africa, Eastern
21 United States, and decreased over the Western United States, South Africa, and semi-arid
22 regions. The correlations of MODIS and AERONET AODs change slightly from 0.928 to
23 0.937 for the C5 and C6 data, respectively. Expected errors for C6 AODs over the Ocean
24 are -0.02 (-10%) and +0.04 (+10%) and over the Land by $\pm (0.05 +15\%)$.

25 **3 Methodology**

26 Figure 1 presents the various regions in the Tropics for which we calculate average IWC
27 profiles. The 12 regions are either over land or ocean since cloud dynamics differs over
28 land and ocean (Houze, 2014) and cloud activity peaks at different local times on a
29 regional basis (Liu and Zipser, 2008). We focus on the Tropics in this study to avoid mid-



1 latitude complications due to frontal dynamics. The 12 regions cover most of the Tropics,
2 yet are limited in longitude, i.e. limited in local times of the A-train observations.

3 An example of the IWC structure of a deep convective cloud, observed near 111° W and
4 8° N on July 10, 2007, is presented in Figure 2. DARDAR IWC, with original units of Kg
5 / m³ is rescaled for graph clarity purposes. 240 individual profiles were measured in this
6 deep convective cloud. In general, IWC increases in value from the top of the cloud
7 downwards, reaches a maximum value, then decreases somewhat. For this cloudy region,
8 latitude and height variations in IWC are apparent, since the heights of the top of the
9 cloud and the maximum IWC values vary as a function of latitude.

10 Based upon the original DARDAR data files, we proceed in several steps, processing
11 both day and night profiles. We first process the DARDAR data into daily files of IWC
12 profiles. An original profile is retained if the profile has IWC greater than 5×10^{-5} Kg /
13 m³ and less than 0.05 Kg / m³ (i.e. near the high end of the retrieval) and if the IWC
14 values are contiguous for two or more kilometers in vertical extent. This Step 1
15 processing is helpful due to the large data volume (i.e. 1.9 TB, 8.2×10^6 profiles for the
16 Tropics) of the original DARDAR data files.

17 The Step 2 processing of the DARDAR and AOD data produces yearly files of deep
18 convective cloud structure for 2007 – 2010. Step 1 profiles are used if the vertical depth
19 of the profile is at least 5 km above 5 km altitude. Step 1 IWC profiles are collocated
20 with the daily MODIS AOD files to calculate IWC_{sum} profile sums binned according to
21 AOD, longitude, latitude, aerosol to cloud pixel distance, season, and altitude. There are
22 three MODIS AOD bins, 72 longitude and 11 latitude bins at 5° resolution, four cloud-
23 screening cases (for “all AOD”, 2, 4, and 6 pixel-distance cases), four seasons, and 131
24 altitude steps in 0.1 km increments from 5 to 18 km altitude. The three AOD bins (i.e.
25 0.05 - 0.15, 0.15-0.35, 0.35 – 0.45), were chosen to represent low, medium, and high
26 amounts of AODs. Calculation of probability distribution functions of AODs (not shown)
27 indicated that there are relatively few MODIS AODs greater than 0.45.



1 The third Step of the processing sorts the IWC_{sum} data into IWC_{reg} averages, binned
2 according to AOD, region, aerosol to cloud pixel distance, season, and altitude. This
3 calculation averages data into seven altitude bins of 2 km vertical extent from 5 to 18 km
4 altitude. The reason for the vertical binning is to promote as much statistical significance
5 as possible from the averaging process. The number of IWC profiles in a single region
6 and altitude bin varies from less than 10^3 to greater than 9×10^4 since AODs are
7 generally smaller over the oceans and the regions vary in spatial extent.

8 We also calculate the *shape* IWC_{shape} of the IWC_{reg} profiles by dividing the IWC_{reg}
9 profile by the IWC_{reg} value in the 5 to 7 km bin range. The IWC_{shape} array has the same
10 binning as the IWC_{reg} array. The IWC_{shape} profile is of course 1.0 for the 5-7 km bin, and
11 deviates from unity at higher altitudes, indicating how the shape of the IWC structure
12 progressively changes above 7 km altitude. As noted above, the calculation of the
13 IWC_{shape} profiles is motivated by the profiles displayed in Figure 6 of Lebo and Seinfeld
14 (2011) since modeled IWC profiles for the three model CCN values diverge at altitudes
15 greater than 5 altitude.

16 Another reason to look at the shape of IWC structure is that observational sampling of a
17 cloudy region for the three AOD bins is not a precisely “controlled” process. A cloudy
18 region has a 3D IWC structure with 3D variations in IWC. The CloudSat and CALIPSO
19 sampling of 3D IWC structures (i.e. a vertical 2D slice through the cloudy region, with a
20 corresponding set of $1^\circ \times 1^\circ$ MODIS AODs) is random. One random sampling of a cloudy
21 region could be weighted by more observations with lower IWC values, and another
22 random sampling could be weighted by higher IWC values. If the sampling of a 3D
23 cloudy region, with respect to low and high regions of IWC, is not consistently similar
24 for the three bins of AOD, then a sampling issue arises. By looking at the shape of the
25 vertical IWC structure one can attempt to mitigate this sampling issue, by putting the
26 IWC_{reg} average profiles for the three AOD bins on a normalized footing. It is reasonable
27 to assume that this sampling issue becomes less of a concern when the number of profiles
28 in a given region and season increases.



1 In Step 4 of the processing, derivatives are calculated two ways. $\partial IWC_{\text{reg}} / \partial AOD$
2 derivatives (henceforth, IWC_{reg} derivatives) are first calculated for each region, season,
3 and pixel-distance AOD field at each of the seven altitude bins. The value of the IWC_{reg}
4 derivative is the average of two derivatives, based upon IWC_{reg} values at the first and
5 second, and first and third, aerosol bins. This average derivative is then transformed, for
6 graphical and other purposes, into percent change in IWC per 0.1 AOD units. In the
7 second calculation, $\partial IWC_{\text{shape}} / \partial AOD$ derivatives are calculated for the seven altitude
8 bins in similar fashion.

9 In Step 5 of the processing, we place the IWC_{reg} derivatives for the various regions and
10 seasons into probability distribution functions (PDFs) at each of the seven altitude bins.
11 Derivatives are included in the PDF if the number of IWC profiles in a derivative is
12 greater than 10^3 . (The 10^3 threshold was empirically determined based upon visual
13 examination of IWC_{reg} profiles). We calculate the means of the PDFs, standard
14 deviations from the means, and 95% (2σ) confidence levels of the means of the PDFs. In
15 a similar manner, the IWC_{shape} derivatives are used to calculate the means of PDFs and
16 95% confidence limits of the means of the PDFs. As discussed below, we examine and
17 compare the means of the two sets of PDFs.

18 Finally, an additional separate processing goes back to Step 2 and assigns AODs at a
19 given $1^\circ \times 1^\circ$ grid box to the AOD at that position using a *randomly* chosen day during the
20 year of interest. Ideally, random AODs should yield means of the PDF of the derivatives
21 that are close to zero, since the $\partial IWC_{\text{reg}} / \partial AOD$ and $\partial IWC_{\text{shape}} / \partial AOD$ derivatives are
22 reversed in sign if low and high values of AOD are interchanged. We compare the PDF
23 means of this separate processing with those of the previous paragraph.

24

25 **4 Results**

26 Figure 3 illustrates the average vertical structure of IWC_{reg} over Africa during summer
27 (June-July-August) and over the southeast Pacific during winter (December-January-



1 February). The mark at 5 km specifies the average between 5 and 7 km altitude, etc. The
2 IWC_{reg} values over Africa increase as AOD increases for nearly every altitude level. In
3 contrast, the IWC_{reg} curves over the southeast Pacific increase from the first to second
4 bin for the 5 to 9 km range, while decreasing for the first and third aerosol bins. These
5 curves illustrate that derivatives for specific regions and seasons can be either positive or
6 negative.

7 These curves also indicate that calculations of derivatives need to be confined to specific
8 regions. There are height differences at which a specific IWC value is observed, e.g. $0.3 \text{ g} / \text{m}^3$
9 occurs at 11 km over the SE Pacific and at 10.5 km over Africa for the 0.01 – 0.15
10 AOD bin. Global calculations which lump together profiles from different regions mix
11 IWC profiles of different height characteristics, due to regional differences in e.g. cloud
12 type and/or weather conditions. If the number of regional profiles varies from region to
13 region for a specific AOD bin, and these profiles have different average height
14 characteristics, then the derivatives calculated using the globally lumped profiles are
15 prone to error (since differences in the average regional profiles are related to both AOD
16 effects and regional differences due to cloud type and/or weather conditions).

17 The impact of cloud adjacency effects upon the AOD fields is illustrated in Figure 4.
18 Daily MODIS C6 AOD data fields were averaged for 25°S to 25°N for “all AOD”, 2, 4,
19 and 6 pixel-distance cases. On the x axis the AODs correspond to the case when all
20 AODs in the $1^\circ \times 1^\circ$ grid box are used to define the AOD field. On the y axis is the ratio of
21 the AODs for a particular pixel-distance to the “all AOD” case. The ratios for all of the
22 curves are smallest for the smaller AODs, and increase to larger values as the AODs
23 increase. The AODs are approximately 2% smaller for the 2 pixel-distance case
24 compared to the “all AOD” case. As more and more AODs are tossed out of the
25 screening process, the AOD averages become progressively smaller than the “all AOD”
26 case, up to 8% for the 6 pixel-distance case. Unfortunately, the number of nonzero $1^\circ \times 1^\circ$
27 grid box AODs decreases for the 4 and 6 pixel-distance cases. Use of the 2 pixel-distance
28 field is more practical than the other cases. Since each AOD bin range in our Step 2
29 binning processing covers a large range in AOD, a 2% effect likely places an “all AOD”
30 and e.g. “2 cloud pixel distance” AOD into the *same* AOD bin range. It is therefore



1 expected that correction for the cloud adjacency effect, using the three AOD bin ranges
2 mentioned above in Section 3, will be of second order in our calculations.

3 In Figure 5 the statistical distribution of IWC_{reg} derivatives for individual regions and
4 seasons, are displayed separately over land and ocean. The x axis indicates the number of
5 individual profiles associated with the derivative, with IWC_{reg} derivatives on the y axis.
6 The absolute magnitude of the derivatives over land or ocean decrease as the number of
7 profiles increases. The largest derivatives are those over mainland India, which are
8 assigned the square symbol in Figure 5. The India land region has the smallest area of our
9 12 regions.

10 Table 1 presents means of the PDFs for the IWC_{reg} derivatives over land and ocean for
11 the 2 km altitude bins, expressed as a function of the pixel-distance value. The means are
12 calculated assigning equal weight to each region (i.e. the calculations are not weighted by
13 the number of profiles observed in each region). The number of statistically significant
14 derivatives (i.e. number of separate regions and seasons) that went into the PDF
15 decreases as the cloud pixel-distance value increases (since the number of AODs in the
16 daily $1^\circ \times 1^\circ$ grid boxes decreases as the pixel-distance value increases). The PDF means
17 are larger over land than the ocean, with fairly small modulation in these means due to
18 pixel-distance choice. Overall, it is apparent that the 3D cloud adjacency effect has a
19 fairly small impact upon the means of the PDFs in our calculations. For this reason, we
20 focus on results for the “all AOD” case in order to maximize the number of derivatives
21 used in our calculations.

22 The means of the IWC_{reg} derivative PDFs for the “all AOD” case are presented in Figure
23 6. The 95% confidence limits of the means are given by the horizontal lines. Over the
24 ocean, the left panel of Figure 6 indicates that the means are consistent with the zero %
25 per 0.1 AOD line, as the zero % line falls between the 95% confidence limits of the
26 means. Over land the means are between 10 and 20 percent for the 9 to 13 km range, also
27 consistent with the 0% line.



1 Table 2 presents means of the PDFs for the IWC_{reg} and IWC_{shape} derivatives over land
2 and ocean for the 2km altitude bins, for the “all AOD” case. As before (see Table 1) the
3 PDF IWCs derivative means over the land are larger than those over the ocean, and the
4 values increase with altitude. In addition, the columns Rnd refer to calculations in which
5 a random day is calculated for each specific day, injecting a random AOD field into the
6 calculations. If AODs are randomly selected from the MODIS AODs, then the final
7 means of the PDFs of the IWC_{shape} derivatives are small, though nonzero. We interpret
8 the nonzero values near 2% as evidence that the means of the *cloud dynamic* variables
9 (e.g. surface humidity, CAPE, surface temperature, etc) are different for the various AOD
10 bins. The fact that the differences in the IWC_{shape} and Rnd columns are positive
11 (especially for the observations over land) indicates, however, that the cloud invigoration
12 effect is nonzero and positive.

13 Examination of individual derivatives over the ocean and land for the various altitude
14 ranges indicates that most regions have positive and negative derivatives. This is
15 consistent with our statements above in the Introduction that buoyancy is perturbed by
16 both positive (latent heat) and negative (condensate loading) influences. There are more
17 positive ocean IWC_{reg} derivatives north than south of the equator, with the largest
18 annually averaged derivatives over the Northwest and Northeast Pacific, and smallest
19 derivatives over the South Atlantic. Largest annually averaged land derivatives are found
20 over India, South America, and Africa, with smallest derivatives over Australia.

21 The means of the IWC_{shape} derivative PDFs for the “all AOD” case are presented in
22 Figure 7. Over the ocean and land the means are near 5% and 10% - 20% per 0.1 AOD
23 for the 9 to 13 km range, respectively. The derivatives are positive to the 2σ level for the
24 9 -11 and 13-15 km altitude ranges over land (i.e. mean - 95% confidence limit of the
25 mean value is positive for these two altitude ranges).

26 As remarked above, in regard to Figure 5, the India averages have a much smaller
27 number of profiles than that for other regions, since the geographical extent of this region
28 is the smallest of the 12 regions. The IWC_{shape} curves are noisier than those of the other



1 regions and the derivatives are substantially larger than those for the other regions. For
2 this reason, it is appropriate to present calculations in which the India land derivatives are
3 excluded. Figure 8 presents calculations, similar to Figure 7, except that the India land
4 derivatives are excluded from the calculation. Over the ocean and land the means are near
5 5% and 4% per 0.1 AOD, respectively, for the 9 - 13 km range.

6 Curves similar to Figure 8 (not shown), were calculated for each Season of the year. Over
7 land the Winter and Spring curves of the IWC_{shape} means have altitude structure similar
8 to Figure 8 in that the means steadily increase as altitude increases. The Fall land means,
9 however, are all near zero. Over the oceans the means are positive above 11 km altitude
10 for all four seasons. The land and ocean seasonal means, however, are not statistically
11 significant to the 2σ level.

12 An alternative way to calculate the means in Figure 8 is to weight the averaging process
13 by the number of profiles in each region. This calculation, which includes India
14 derivatives (but gives them little weight), again yields means between 5% and 4% per 0.1
15 AOD over ocean and land, respectively.

16 Finally, Figure 9 displays the means of PDFs specified by combining the land and ocean
17 IWC_{shape} derivatives, excluding the India land derivatives, to obtain a *Tropical average*.
18 The means are near 5% per 0.1 AOD (as expected from Figure 8), and positive to the 2σ
19 level in the 11 to 15 km altitude range. Also displayed in Figure 9 are means calculated
20 using the IWC_{reg} derivatives, again excluding the India land derivatives. The means are
21 positive above 9 km altitude, but not statistically significant at the 2σ level. The mean in
22 the 5-7 km altitude range is nonzero (i.e. 0.04) but very small.

23 **5 Discussion**

24 The calculations above are supportive of a small positive signed cloud invigoration
25 effect. IWC increases slightly on average for deep convective clouds above the freezing
26 level as AODs increase. The Figure 7 means of the IWC_{shape} PDF, based upon all
27 Tropical regions, indicates mean IWC_{shape} derivatives over the ocean and land are near



1 5% and 10-20% per 0.1 AOD in the 9 -13 km altitude range, respectively. The derivatives
2 are positive to the 2σ level for the 9-11 and 13-15 km altitude ranges over land. If the
3 largest derivatives (see Figure 5, those over India), are excluded from the processing
4 (since the India derivatives are very much larger than the other derivatives, and many less
5 cloudy scenes are observed over India due to the comparatively smaller geographical size
6 of India), then the IWC_{shape} land mean derivative is near 4% (see Figure 8).

7 The Tropical average means (Figure 9), calculated using combined ocean and land
8 IWC_{shape} derivatives (excluding mainland India) are near 5% per 0.1 AOD above 9 km
9 altitude, and positive to the 2σ level in the 11 – 15 km range. The 5% per 0.1 AOD value
10 is similar to the observed 7% per 0.1 AOD value (corresponding to the cloud top pressure
11 data of Figure 6 from Koren et al., 2010), and similar to the 3% – 5% increase in medium
12 and high cloud tops calculated by Storer and van den Heever (2013), but substantially
13 less than the $\sim 127\%$ / 0.1 AOD change in the IWC profile indicated by the bin
14 microphysics calculations presented in Figure 6 of Lebo and Seinfeld (2011).

15 As discussed above, the IWC_{reg} average profiles are calculated without normalization at 5
16 km altitude. The IWC_{reg} means (excluding India) are positive above 9 km but not
17 statistically significant at the 2σ level. The lack of statistical significance is similar to the
18 conclusions of Wall, Zipser, and Liu (2014). One is struck by the fact that our study and
19 that of Wall, Zipser, and Liu (2014) both yield small aerosol indirect effects when many
20 years of data are processed.

21 Generally, Figure 5 imparts an important lesson – the scatter in the measured derivatives
22 decreases for a region when the number of observed profiles in the region increases. We
23 interpret Figure 5 as follows. Changes in IWC vertical structure are due to both aerosol
24 and cloud dynamic influences. For a specific region, a relatively small number of profiles
25 will not likely sample the PDFs of all variables (aerosol and cloud dynamic variables
26 such as surface and 500 hPa relative humidity, CAPE, wind shear, etc) as completely as
27 for the case in which a larger number of profiles are considered. Differences in the
28 average IWC_{reg} profiles at different AODs can be due to differences in cloud dynamic



1 differences, to a greater extent than to the AOD difference, depending upon
2 circumstance, if the number of observed profiles is relatively small. A negative (or large
3 positive) derivative could be due to a change in cloud dynamic influences and not the
4 AOD change. In addition, the CloudSat/CALIPSO observational “curtains” slice through
5 a cloudy region. If the sampling of the 3D cloudy regions with respect to low and high
6 regions of IWC is not consistently similar for the e.g. three bins of AOD, then a sampling
7 issue arises. This sampling consideration becomes less of an issue when the number of
8 observed profiles increases.

9 Interest in the cloud invigoration process is of course important due to its consequences
10 in regard to the radiative effects of aerosol indirect effects – perturbations in cloud
11 vertical structure due to changes in aerosol translate into perturbations in the radiative
12 effects of clouds upon climate. Understanding the effects of aerosols upon cloud structure
13 is a necessary step towards understanding the radiative effects. Global calculations which
14 average regional and seasonal perturbations of cloud structure over many years are of
15 interest since they yield a grand ensemble average that fully samples the PDFs of the
16 aerosol and cloud dynamic variables.

17 Cloud adjacency (i.e. 3D radiative transfer) issues are real, but the impact in our
18 calculations is a second order effect. The 3D cloud adjacency effects appear not to be a
19 major impediment in regard to calculation of aerosol-cloud indirect effects, if the AOD
20 bin ranges are fairly wide compared to the size of the 3D effect (see Figure 4). The
21 variations in the IWC_{reg} land derivatives in Table 1 for the “all AOD”, 2, 4 pixel-unit
22 cases is much smaller than the altitude variations in the derivatives. We place an AOD
23 into one of three AOD bin ranges. An e.g. 2% AOD correction (see Figure 4) due to
24 cloud adjacency effects does not likely move the AOD from one bin range to another. As
25 remarked above, the number of $1^\circ \times 1^\circ$ AODs decrease as the pixel-distance unit increases,
26 and with the “all AOD” and 2 pixel-distance AODs giving similar derivatives over land
27 in the right-hand portion of Table 1, the necessity to apply the pixel-distance correction is
28 debatable.



1 In conclusion, the literature of observed and modeled aerosol-cloud indirect effects is
2 characterized by a range of results of different signed outcomes, including this study.
3 This is due to the fact that numerous variables and other physical considerations can
4 influence whether a positive or negative effect is measured. For example, absorptive
5 aerosol is known to stabilize the lowermost several kilometers of temperature profiles,
6 and thus could impact cloud development. In our study we consider all MODIS AODs
7 equally, without attention to the type of aerosol (be it predominantly scattering or
8 absorptive in nature). We will address this issue in follow-on calculations, and also
9 extend our calculations to include dynamic variables in the analyses.

10

11 **Acknowledgements**

12 The work discussed in this paper is supported by NASA Grants NNX14AL55G and
13 NNX14AO85G. DARDAR data were provided by NASA/CNES and we thank the
14 ICARE Data and Services Center (<http://www.icare-lille1.fr>) for providing access to the
15 data used in this study. The National Center for Atmospheric Research (NCAR) is
16 supported by the National Science Foundation.

17

18 **References**

19 Cotton, W., and Coauthors: RAMS 2001: Current status and future directions, *Meteor.*
20 *Atmos. Phys.* 82, 5-29, 2003.

21 Delanoë, J., and Hogan, R. J.: A variational scheme for retrieving ice cloud properties
22 from combined radar, lidar, and infrared radiometer, *J. Geophys. Res.*, 113, D07204,
23 doi:10.1029/2007JD009000, 2008.

24 Delanoë, J., and Hogan, R. J.: Combined CloudSat-CALIPSO-MODIS retrievals of the
25 properties of ice clouds, *J. Geophys. Res.*, 115, D00H29, doi:10.1029/2009JD012346,
26 2010.



- 1 Deng, M., Mace, G. G., Wang, Z., and Lawson, P. R.: Evaluation of Several A-Train Ice
2 Cloud Retrieval Products with In Situ Measurements Collected during the SPARTICUS
3 Campaign, *J. Appl. Met. Clim.*, 52, 1014-1030, 2013.
- 4 Hogan, R. J.: Fast approximate calculation of multiply scattered lidar returns, *Appl. Opt.*,
5 45, 5984–5992, 2006.
- 6 Houze, R.: *Cloud Dynamics*, Elsevier, Amsterdam, 2014.
- 7 Koren, I., Feingold, G., and Remer, L. A.: The invigoration of deep convective clouds
8 over the Atlantic: aerosol effect, meteorology or retrieval artifact? *Atmos. Chem. Phys.*,
9 10, 8855-8872, 2010.
- 10 Lebo, Z. J., and Seinfeld, J. H.: Theoretical basis for convective invigoration due to
11 increased aerosol concentration, *Atmos. Chem. Phys.*, 11, 54-7-5429, 2011.
- 12 Levy, R. C., Mattoo, S., Munchak, L. A., Remer, L. A., Sayer, A. M., Patadia, F., and
13 Hsu, N. C.: The Collection 6 MODIS aerosol products over land and ocean, *Atmos.*
14 *Meas. Tech.*, 6, 2989-3034, doi:10.5194/amt-6-2989-2013, 2013.
- 15 Levy, R. C., Mattoo, S., Munchak, L. A., Kleidman, A. R., Patadia, F., and Gupta, P:
16 MODIS Atmosphere Team Webinar Series#2: Overview of Collection 6 Dark-Target
17 aerosol product, http://modis-atmos.gsfc.nasa.gov/products_C006update.html, 2014.
- 18 Liu, C., and Zipser, E. J.: Diurnal cycles of precipitation, clouds, and lightning in the
19 tropics from 9 years of TRMM observations, *Geophys. Res. Lett.*, 35, L04819,
20 doi:10.1029/2007GL032437, 2008.
- 21 Rodgers, C. D: *Inverse Methods for Atmospheric Sounding*. World Scientific, Singapore,
22 2000.
- 23 Rosenfeld, D., Lohmann, U., Raga, G. B, O’Dowd, C. D, Kulmala, M., Fuzzi, S.,
24 Reissell, A., and Andreae, M. O.: Flood or drought: How do aerosols affect
25 precipitation?, *Science*, 321, 1309– 1313, doi:10.1126/science.1160606, 2008.



- 1 Stephens, G. L., Vane, D. G., Boain, R. J., Mace, G. G., Sassen, K., Wang, Z.,
2 Illingworth, A. J., O'Connor, E. J., Rossow, W. B., Durden, S. L., Miller, S. D., Austin,
3 R. T., Benedetti, A., Mitrescu, C., and The CloudSat Science Team: THE CLOUDSAT
4 MISSION AND THE A-TRAIN, *Bull. Amer. Meteor. Soc.*, **83**, 1771–1790, doi:
5 <http://dx.doi.org/10.1175/BAMS-83-12-1771>, 2002.
- 6 Stocker, T.F., Qin, D., Plattner, G.-K., Alexander, L. V., Allen, S. K., Bindoff, N. L.,
7 Bréon, F.-M., Church, J. A., Cubasch, U., Emori, S., Forster, P., Friedlingstein, P.,
8 Gillett, N., Gregory, J. M., Hartmann, D. L., Jansen, E., Kirtman, B., Knutti, R., Krishna
9 Kumar, K., Lemke, P., Marotzke, J., Masson-Delmotte, V., Meehl, G. A., Mokhov, I. I.,
10 Piao, S., Ramaswamy, S. V., Randall, D., Rhein, M., Rojas, M., Sabine, C., Shindell, D.,
11 Talley, L. D., Vaughan, D. G., and Xie, S.-P.: Technical Summary. In: *Climate Change*
12 *2013: The Physical Science Basis. Contribution of Working Group I to the Fifth Assess-*
13 *ment Report of the Intergovernmental Panel on Climate Change* [Stocker, T.F., Qin, D.,
14 Plattner, G.-K., Tignor, M., Allen, S. K., Boschung, J., Nauels, A., Xia, Y., Bex, V., and
15 Midgley, P. M. (eds.)]. Cambridge University Press, Cambridge, United Kingdom and
16 New York, NY, USA, 2013.
- 17 Storer, R. L., and van den Heever, S. C.: Microphysical Processes Evident in Aerosol
18 Forcing of Tropical Deep Convective Clouds, *J. Atm. Sci.*, **70**, 430-446, 2013.
- 19 Tao, W.-K., Chen, J.-P., Li, Z., Wang, C., and Zhang, C.: Impact of aerosols on
20 convective clouds and precipitation, *Rev. Geophys.*, **50**, RG2001, doi:10.1029
21 /2011RG000369, 2012.
- 22 Wall, C., Zipser, E., and Liu, C.: An Investigation of the Aerosol Indirect Effect on
23 convective Intensity Using Satellite Observations, *J. Atmos. Sci.*, **71**, 430-447, 2014.
- 24 Winker, D. M., Pelon, J., Coakley Jr., J. A., Ackerman, S. A., Charlson, R. J., Colarco, P.
25 R., Flamant, P., Fu, Q., Hoff, R. M., Kittaka, C., Kubar, T. L., Le Treut, H., McCormick,
26 M. P., Mégie, G., Poole, L., Powell, K., Trepte, C., Vaughan, M. A., and Wielicki, B. A.:
27 The CALIPSO Mission: A Global 3D View of Aerosols and Clouds. *Bull. Amer. Meteor.*
28 *Soc.*, **91**, 1211–1229. doi: <http://dx.doi.org/10.1175/2010BAMS3009.1> , 2010.



- 1 Varnai, T., and Marshak, A.: MODIS observations of enhanced clear sky reflectance near
- 2 clouds, *Geophys. Res. Lett.*, 36, L06807, doi:10.1029/2008GL037089, 2009.

- 3 Zhang, J., Reid, J. S., and Holben, B. N.: An analysis of potential cloud artifacts in
- 4 MODIS over ocean aerosol optical thickness products, *Geophys. Res. Lett.*, 32, L15803,
- 5 doi:10.1029/2005GL023254, 2005.



1 Table 1. Average IWC_{reg} derivatives over ocean and land (in % / 0.1 AOD units)
 2 expressed as a function of average pixel-distance values used to derive the AOD fields.

3

4 <u>Altitude</u>	5 <u>Ocean</u>			6 <u>Land</u>		
7 (km)	0	2	4 pixels	0	2	4 pixels
8 13-15	4.4	5.1	-3.8	2.8	1.7	1.7
9	(47	42	27)	(31	31	28)
10 11-13	0.6	-0.3	2.8	23.1	23.5	15.8
11	(53	53	46)	(36	36	34)
12 9-11	-0.9	-0.2	-0.5	18.0	18.0	19.1
13	(54	54	48)	(36	36	36)
14 7-9	-1.7	-0.2	0.5	6.4	6.8	6.6
15	(54	55	48)	(36	36	36)
16 5-7	0.4	0.9	1.9	1.7	1.6	1.6
17	(54	54	48)	(36	36	36)

18 2-pixels is for AOD to cloud pixel-distances ≥ 2

19 Numbers in () are the number of regional and seasonal derivatives used to define the
 20 averages.



1 Table 2. Average IWC_{reg} and IWC_{shape} derivatives over ocean and land (expressed in
2 % change in IWC / 0.1 AOD units)

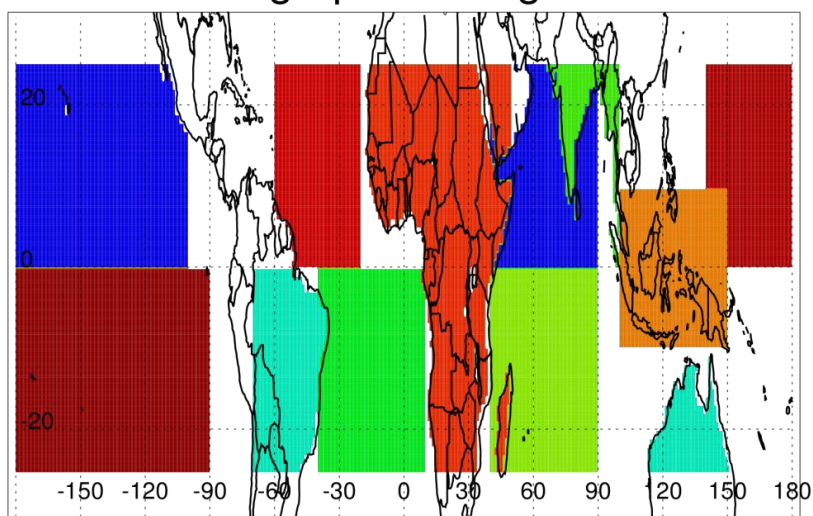
3 _____

4 <u>Altitude</u>	<u>Ocean</u>			<u>Land</u>		
5 (km)	IWC _{reg}	Shape		IWC _{reg}	Shape	
6		IWC _{shape}	Rnd		IWC _{shape}	Rnd
7 _____						
8 13-15	4.4	7.4	2.0	2.8	4.6	1.6
9 11-13	0.6	5.3	2.8	23.1	23.8	1.2
10 9-11	-0.9	5.4	2.1	18.0	14.5	0.1
11 7-9	-1.7	-0.2	1.2	6.5	3.0	-0.7
12 5-7	0.4	0.0	0.0	1.7	0.0	0.0
13 _____						

14 Rnd – same as IWC_{shape}, with random MODIS AOD values used in the calculation.

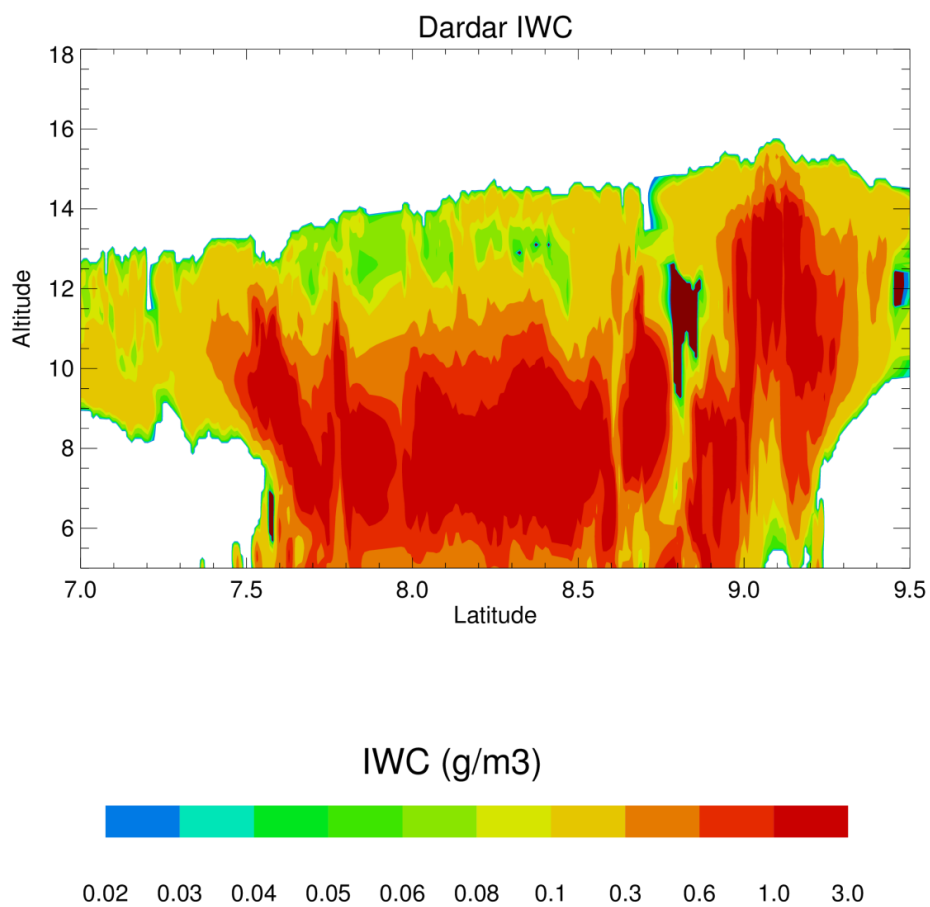


Geographical Regions



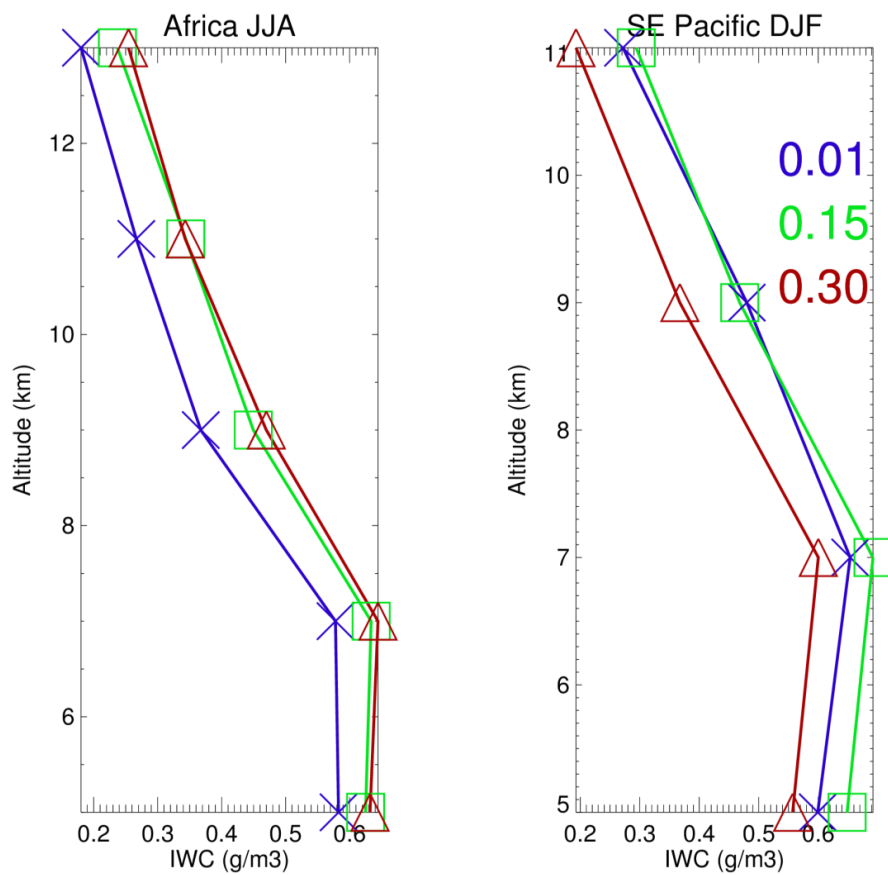
1

2 Figure 1. Geographical Tropical regions over land and ocean.



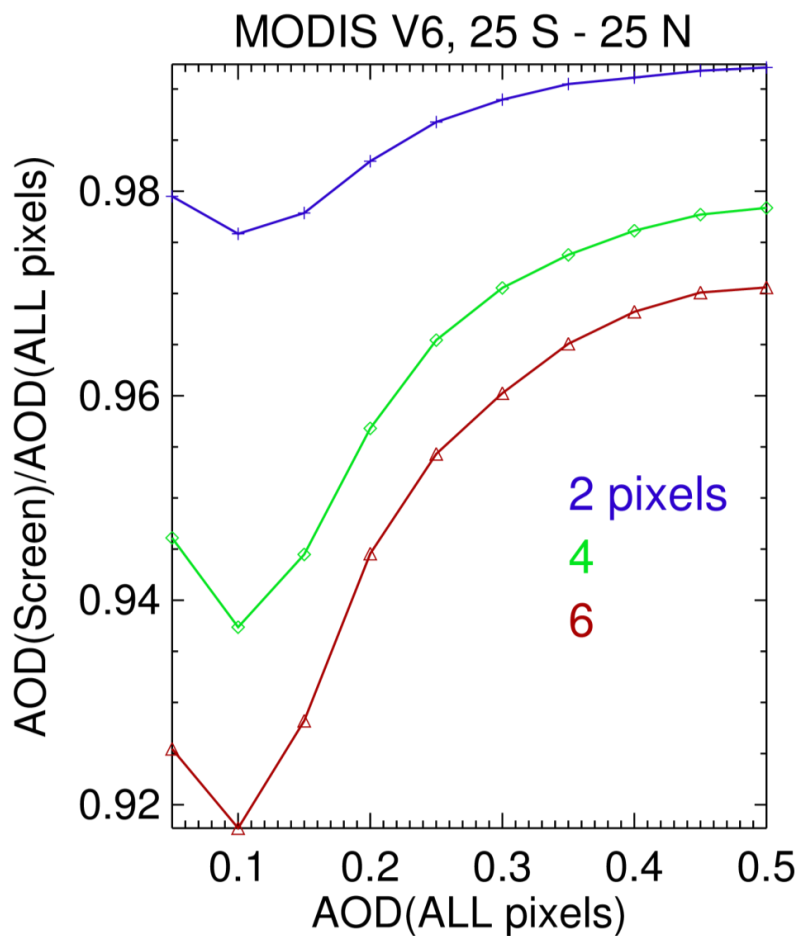
1

2 Figure 2. DARDAR IWC structure of a tropical cloudy region observed on July 10, 2007.



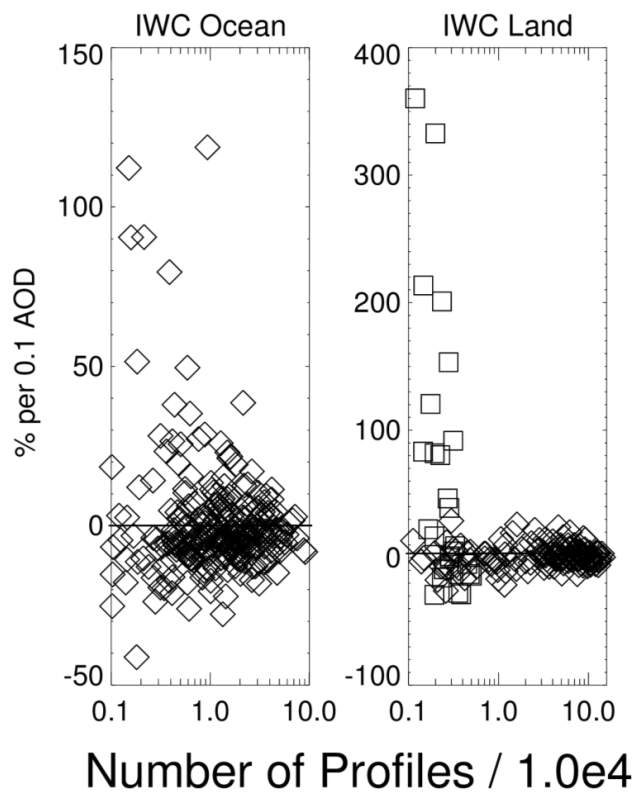
1

2 Figure 3. Average IWC_{reg} vertical profiles over SE Pacific during December-January-
3 February and over Africa during June-July-August for MODIS aerosol bins with lower
4 bin limits of 0.01, 0.15, and 0.30. Data has been averaged into 2 km bins of vertical
5 altitude.



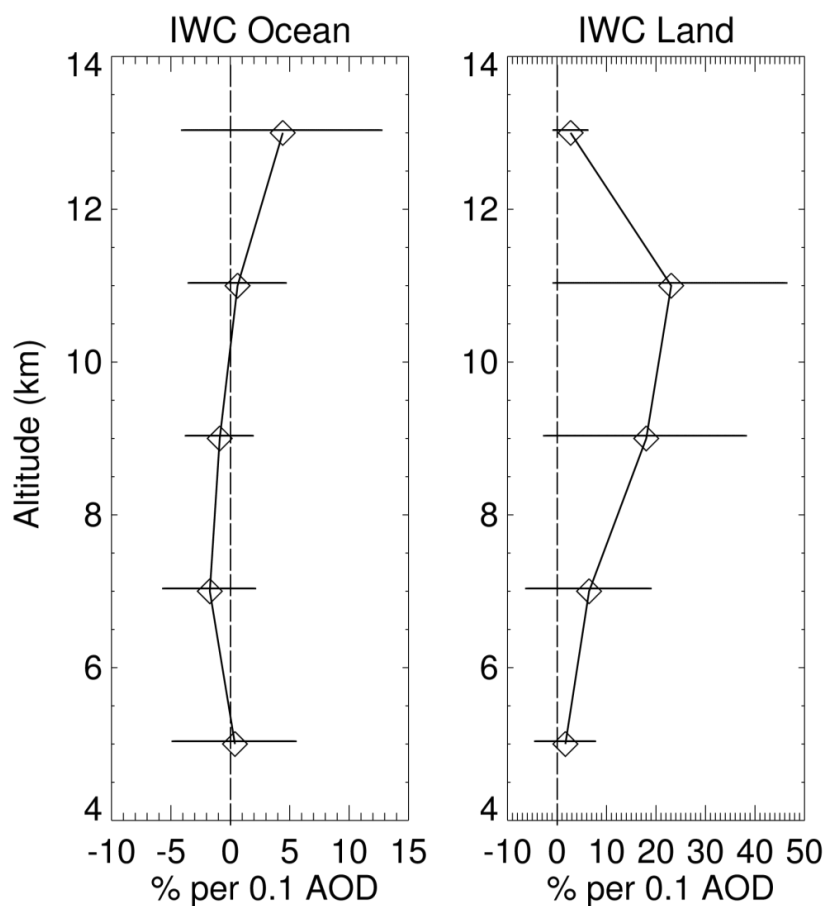
1

2 Figure 4. Curves of $1^\circ \times 1^\circ$ MODIS V6 AOD averages, calculated with and without cloud
3 pixel-distance screening. X axis AOD values are calculated using all MODIS AOD data,
4 and Y axis AODs are calculated by averaging AODs such that the AODs in the $1^\circ \times 1^\circ$
5 geographical area are at 2, 4, and 6 pixel-distances from clouds. Data from 2007 – 2010,
6 for $25^\circ \text{ S} - 25^\circ \text{ N}$, is used.



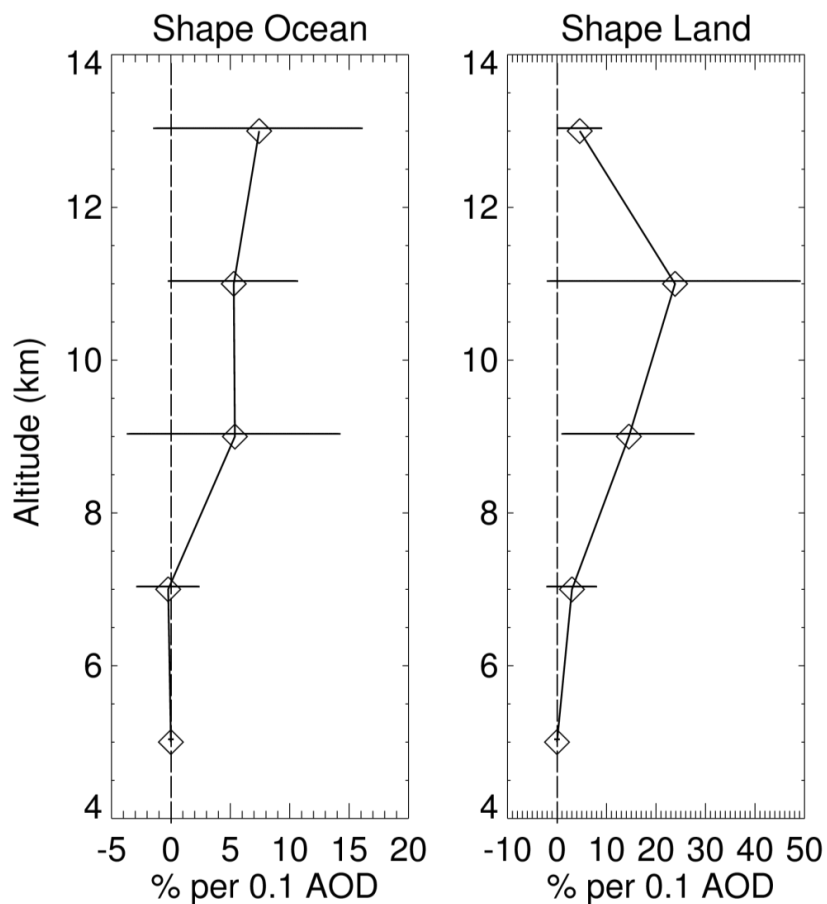
1

2 Figure 5. Statistical distribution of IWC_{reg} derivatives between 5 and 15 km altitude for
3 individual regions and seasons as a function of the number of profiles used to define each
4 derivative. Derivatives over mainland India are assigned a square symbol.



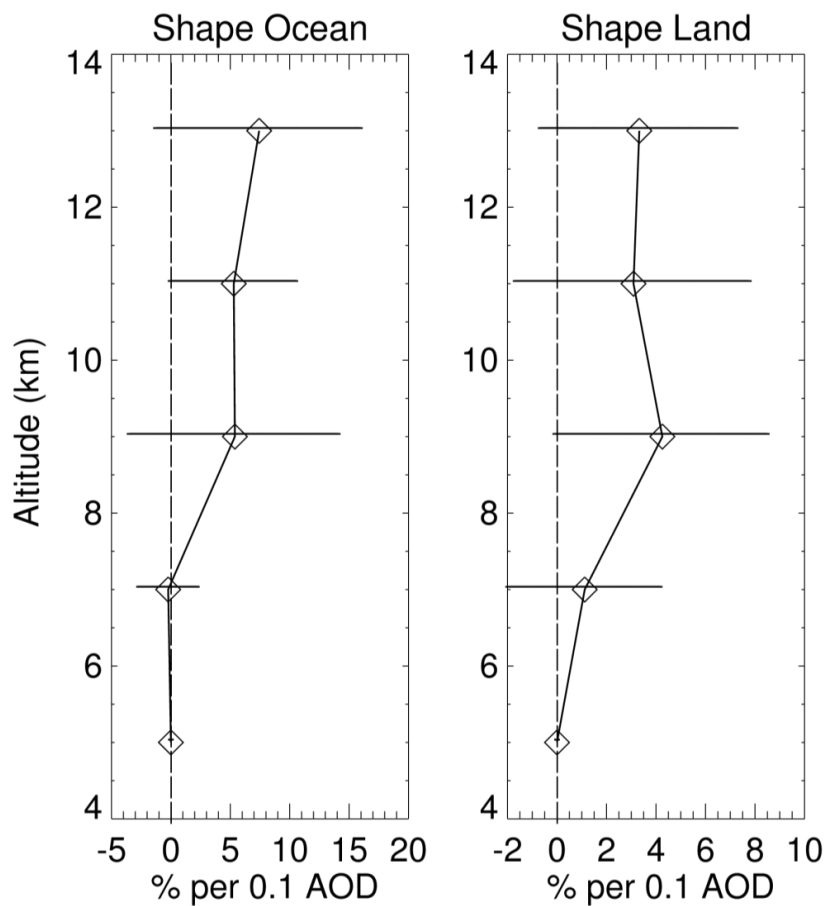
1

2 Figure 6. Vertical profiles of the means of the PDFs of IWC_{reg} derivatives for individual
3 regions and seasons based upon DARDAR IWC profiles, and MODIS AOD data for the
4 “all AOD” case. Mean 95% confidence limits are indicated by the horizontal lines. The
5 symbol at 5 km denotes the average for the 5-7 km altitude range.



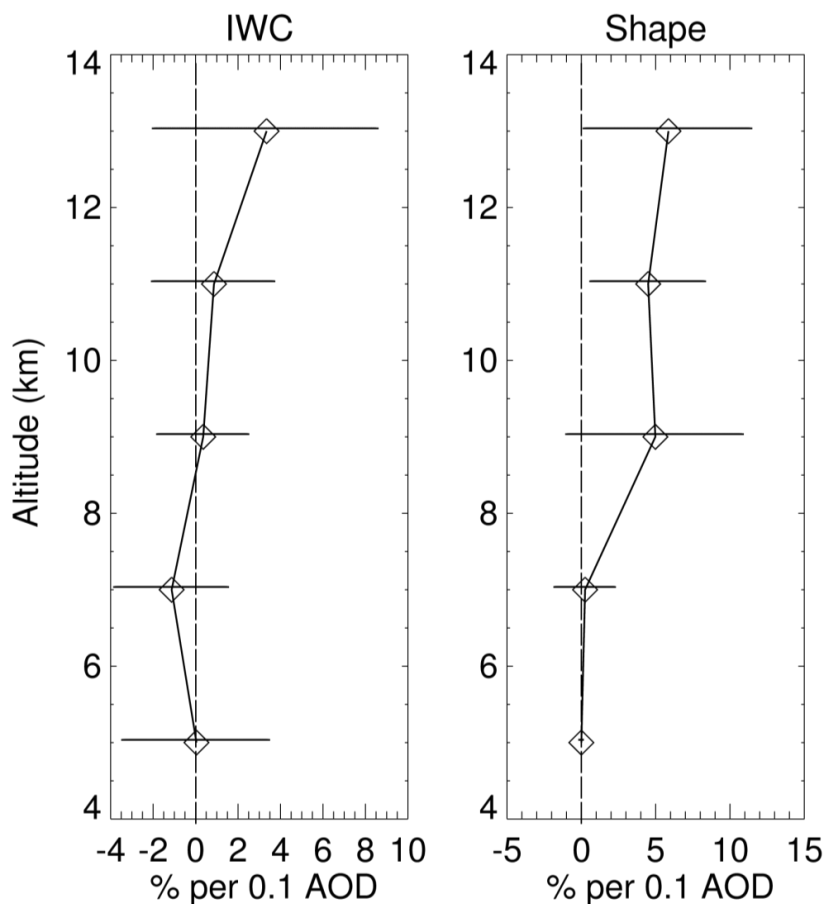
1

- 2 Figure 7. Vertical profiles of the means of the IWC_{shape} regional and seasonal derivatives.
3 MODIS “all AOD” data are used. Mean 95% confidence limits are indicated by the
4 horizontal lines.



1

2 Figure 8. Same as Figure 7 except that India land IWC_{shape} derivatives are excluded from
3 the averaging process.



1

2 Figure 9. Means of PDFs of IWC_{reg} and IWC_{shape} derivatives over ocean and land,
3 excluding India land derivatives. Mean 95% confidence limits, given by the horizontal
4 lines, indicate that IWC_{shape} means are positive to the 2σ level for the 11–15 km altitude
5 range.